



## City Research Online

### City, University of London Institutional Repository

---

**Citation:** Midmer, A. & Bruecker, C. (2022). Nature-inspired self-adaptive wingtip for vortex mitigation. *The Aeronautical Journal*, ISSN 0001-9240

This is the accepted version of the paper.

This version of the publication may differ from the final published version.

---

**Permanent repository link:** <https://openaccess.city.ac.uk/id/eprint/29084/>

**Link to published version:**

**Copyright:** City Research Online aims to make research outputs of City, University of London available to a wider audience. Copyright and Moral Rights remain with the author(s) and/or copyright holders. URLs from City Research Online may be freely distributed and linked to.

**Reuse:** Copies of full items can be used for personal research or study, educational, or not-for-profit purposes without prior permission or charge. Provided that the authors, title and full bibliographic details are credited, a hyperlink and/or URL is given for the original metadata page and the content is not changed in any way.

## Nature-inspired self-adaptive wingtip for vortex mitigation

Alden Midmer  
alden.midmer@city.ac.uk

Professor Christoph Bruecker  
christoph.bruecker@city.ac.uk

**Abstract**

Flexible wingtip extensions attached to the end of a symmetric (NACA 0012) aerofoil have been tested at  $0^\circ$ ,  $5^\circ$ ,  $10^\circ$  angles of attack and speeds of  $20 \text{ cm s}^{-1}$ ,  $30 \text{ cm s}^{-1}$ ,  $40 \text{ cm s}^{-1}$ . Time resolved particle image velocimetry (TR-PIV) was used to compare a clean wing and a wing with flexible wingtip extensions. Material testing of the extensions were also conducted to ensure comparable flow conditions between that of bird flight and the tests. As anticipated for the clean wing, a large roll-up motion was observed which resulted in a large wingtip vortex. However when the flexible extensions were attached, it has been shown that the main tip vortex is dislocated and separated into smaller vortices off of each tip. It is concluded that the flexible extensions are able to replicate a bird's slotted wingtip and modify the vortex sheet to reduce induced drag.

**Nomenclature**

Symbol	Units	Description
$a_k$	-	$k^{th}$ Eigen mode
$C_l$	-	Lift coefficient
$C_y$	-	Cauchy number
$E$	GPa	Young's Modulus
$f$	Hz	Vibration frequency
$I$	$\text{m}^4$	Second moment of area
$L$	m	Flaplet length
PLA	-	Poly Lactic Acid
$R_c$	-	Chord Reynolds number
$T$	m	Flaplet thickness
TPU	-	Thermoplastic Polyurethane
$U$	$\text{cm s}^{-1}$	Mean flow
$W$	m	Flaplet width
$\rho_f$	$\text{kg m}^{-3}$	Flaplet density
$\rho_w$	$\text{kg m}^{-3}$	Water density

**1 Introduction**

A contributor to the overall aeroacoustic noise and aerodynamic inefficiency of a lifting body is the roll-up motion that occurs at the wingtip. To improve the aerodynamic performance of a wing there are many forms of wingtip devices, such as winglets and sharklets, that reduce the influence of induced drag. In this present study, flexible wing-end extensions mimicking the primary feathers of a birds wingtip have been tested.

Some species of birds, particularly those that glide for extended periods, have evolved to have split wingtip feathers. The purpose of this adaptation was presumed to mostly improve aerody-

dynamic efficiency (Withers 1981). A study conducted by KleinHeerenbrink, Johansson, and Hedenström 2017 on the effects of a jackdaw's slotted wingtip demonstrated the spreading of vorticity and the benefits of a slotted wingtip to improve span efficiency; whereby a slotted wingtip could improve the span efficiency by up to 6.6% when compared to an optimal planar wing. The benefits of spreading wingtip vorticity was studied by Tucker 1993 who compared a base wing with a Clark - Y aerofoil and a feathered extension. Concluding that the slotted (feathered) wingtip could have a drag reduction of 12% due to the spreading of the vortex sheet when compared to a planar wing. Further theoretical studies on static non-planar wingtips (Cone 1962) have concluded that when used they can improve aerodynamic efficiency however, in order to maintain optimal wing loading the wingtip must be able to change geometry. Other potential benefits of a slotted wingtip have been studied by Wissa, Han, and Cutkosky 2015 in which the wingtip feathers were latched together in normal conditions and separated under abnormal conditions. It was found that when separated the slots could alleviate gust loads and delay the onset of stall. This study build off previous research in order to explore the potential benefits of flexible extensions on the wingtip. Prior studies have shown that the spreading of vorticity is able to reduce induced drag and therefore the total drag of an aerofoil, however there have been no studies on the use of flexible self-adaptive wingtips on vortex spreading.

**2 Looking to nature**

Initially a  $1^{st}$  order model will be used to mimic a birds split wingtip feathers, which would result in the simplification of the complex geometry, cross sec-



Figure 1: Peregrine Falcon's split wingtip (Dudley 2016)

tion and variable spanwise rigidity of the feathers. In reducing the complexity the ability to mimic the self-adaptive characteristic of a birds split wingtip solely on effects of the slots and flexible extensions can be analysed. To allow for a proper comparison between the model and nature similar chord based Reynolds numbers as found in avian flight ( $10^4$ ) will be used during the tests.

For the tests herein the tip section of a Peregrine Falcon's primary feather is used as a basis of modelling.

### 3 Experimental setup

The tests were conducted in the Handley Page Laboratory at City, University of London in the CHB water tunnel. The tunnel is a closed loop with an open surface perspex test section of 0.4 m width, 0.5 m height and a length of 1.2 m.

Time Resolved Particle Image Velocimetry (TR-PIV) measurements were conducted using an LED light sheet, of 5 mm nominal thickness and 550 nm wavelength, positioned normal to the mean flow. The light source used was a Hardsoft IL-105/6X illuminator which was set to continuous wave throughout the tests and was equipped with a convex lens to convert the light beam to a sheet. A Phantom Miro M310 high speed camera (1280 x 800 pixel window size) equipped with a Tokina 100 mm macro lens was used to capture the flow. The images were taken at a sample rate of 250  $f_{ps}$  with an  $f2.8$  and an exposure time of 3900  $\mu s$ . Silver coated ceramic particles, of approximate diameter 50  $\mu m$ , were used as the seeding and placed into the light-sheet between each test run.

Running over the top of the tunnel was a traverse

system which the wing was mounted to. During the experiments, the traverse was used to move the wing along the test section at the desired velocities. For each run, the wing was initially positioned with the leading edge in the light sheet, the wing then passed through the light sheet and to the end of the test section (totalling a 0.9 m traverse distance). The structures normal to the mean flow were observed via a mirror orientated at  $45^\circ$  to the model and positioned downstream on the floor of the tunnel (figure 2). Images were then captured with a high speed camera positioned outside of the tunnel and aligned  $45^\circ$  to the face of the mirror. In each test the camera had the same field of view and remained focused on the middle of the light-sheet. The flow field was recorded from before the wingtip was accelerated, in order to capture the background flow, to when the vortex was observed to have dissipated.

#### 3.1 Wing model

The aerofoil section used was a NACA 0012, with a chord of 300 mm and span of 400 mm. The wing section was hollow and housed within were 5 pneumatic actuators, operated with a control box, connected to each flexible extension to enable the deployment distance to be adjusted. Attached to the wing-end was a rounded wingtip with slots for the wingtip extensions to pass through; the wing and wingtip were then held together with 4 rods, 2 fore and 2 aft. Both the wing and wingtip were 3D printed out of PLA filament on a Creality Ender 3 V2 printer at a 0.12 mm layer height. The flexible extensions were also 3D printed but, using TPU filament on the same aforementioned printer. The use of TPU filament enabled the precise manufacture of extensions that would deform under load and return to its original shape when the load was removed. The flexible extensions were 100 mm long, 20 mm wide, 1.5 mm thick and had an inter-spacing of 10 mm (beginning 40 mm aft of the leading edge). The root of the extensions were unable to twist however, towards the tip twisting could occur due to the nature of the material used.

### 4 Results

Three speeds,  $20 \text{ cm s}^{-1}$ ,  $30 \text{ cm s}^{-1}$  and  $40 \text{ cm s}^{-1}$ , were tested (which correlate to chord based Reynolds numbers of 50,000, 70,000 and 90,000) at  $0^\circ$ ,  $5^\circ$  and  $10^\circ$  angle of attack. All test cases were run with a clean wingtip and flexible extension configuration to allow for comparative analysis. For

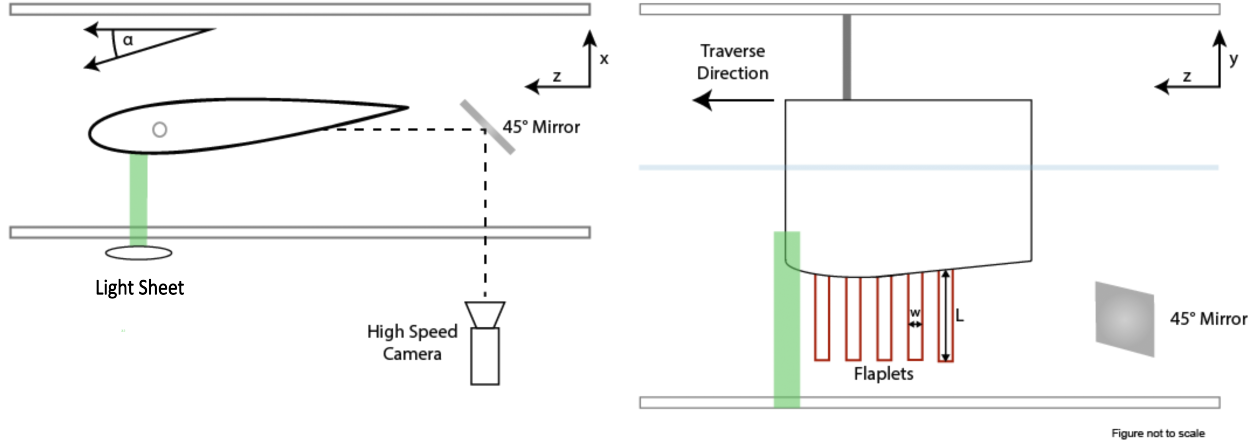


Figure 2: Experimental arrangement

the remainder of the report the  $10^\circ$ ,  $30 \text{ cm s}^{-1}$ ,  $10^\circ$ ,  $20 \text{ cm s}^{-1}$  and  $5^\circ$ ,  $30 \text{ cm s}^{-1}$  tests are shown.

#### 4.1 Flexible extension properties

Due to the nature of the flexible extensions protruding out of the wingtip and their ability to move freely at the tip under the influence of the roll-up motion they can be regarded as thin cantilever beams. To this end the equation of motion can be expressed as (Stanek 1965):

$$EI \frac{\partial^2 w}{\partial x^4} = -\rho A \frac{\partial^2 w}{\partial t^2} - \frac{c}{L} \frac{\partial w}{\partial t} \quad (1)$$

In order to ascertain the Youngs Modulus of the material the natural frequency of the TPU extensions can be used along with applying the condition of no viscous dampening to equation 1. From this the resulting equation 2 is obtained:

$$f = \frac{a_k^2 T}{2\pi L^2} \sqrt{\frac{E}{12\rho}} \quad (2)$$

To find the natural frequency of the wingtip extensions a step-response test was conducted where a single printed piece was displaced from equilibrium and then released. The test piece was clamped vertically at one end and free to oscillate after being displaced; the tip motion was then captured using the same high speed camera mentioned above. The analysis of the tip oscillation was achieved with the addition of a black dot on the tip of the wingtip extension and a MATLAB code which recorded the pixel intensity at the tip equilibrium position. Figure 3 shows the Fast Fourier Transform (FFT) of the pixel intensity and the frequency (8.15 Hz) associated with the first peak. Substituting in the frequency and rearranging equation 2, the Youngs

Modulus was calculated to be 0.196 GPa which is lower than the 7.0 GPa (Schmitz et al. 2015) of a peregrine falcon's primary feather. However, as the flow conditions and fluid in each case is different non-dimensional parameters are required for an accurate comparison.

#### 4.2 Non-dimensional parameters

Using the horizontal displacement and curvature observed from the leading extension during the  $30 \text{ cm s}^{-1}$ ,  $10^\circ$  test, a point load was applied to the free end of a flexible extension clamped horizontally. The equivalent point load to the observed curvature seen during testing can be used, along with the extension's geometry, to find an estimate for the force coefficient (in this experiment  $C_f$ ). The Cauchy number, which is the ratio of the hydrodynamic force and the restoring force due to the wingtip extension stiffness, can be calculated using (Song et al. 2021):

$$C_y = \frac{\rho_w U^2 C_f W L^3}{2EI} \quad (3)$$

In this instance using the test case set out above for the primary extension, the Cauchy number was 0.582. An approximate Cauchy number for a peregrine falcon's primary feather can also be calculated using feather data collected by Schmitz et al. 2015, cruise speed by Cornell Lab of Ornithology 2019, a bird's wingtip  $C_f$  by Tucker 1993 and typical feather mass by Williams 2019. The resulting approximated Cauchy number for the outer 25% of a primary feather (the region that exhibits the most bending) is 0.593, suggesting the flexible extensions in this experiment will behave similarly to a falcon's primary feather.

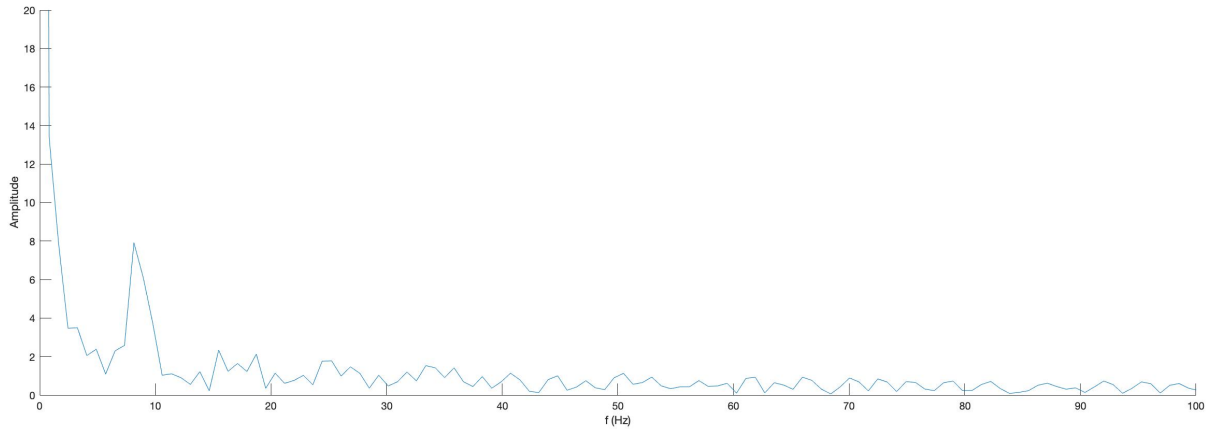


Figure 3: FFT

### 4.3 Flow visualisation

Figure 4 shows the flow visualisation for the 30 cm,  $10^\circ$  clean and flexible extension wingtips taken directly from the raw camera images. In each instance, the visualisation was taken when the vortex core was fully developed off the tips and downstream of the wing section. The multi-exposure snapshots are combination of 10 images with an inter-spacing of two images (12 ms apart) stacked together on Adobe Photoshop. The vortex cores for the clean and flexible extension wingtip are easily identifiable and are estimated to be (from the flow visualisation and review of the raw footage) 45 mm for the clean wingtip, 35 mm and 30 mm for the  $30 \text{ cm s}^{-1}$  and  $20 \text{ cm s}^{-1}$  respectively. From the flow visualisation alone it is clear how the addition of the flexible extensions have not only reduced the size of the vortex relative to the clean wingtip, but also dislocated it further away from the wing.

### 4.4 Processing method

The captured images were processed using an in house MATLAB code which uses a classical 2D cross correlation method and post processing. Two passes of the images were conducted with a 50% overlap, where the interrogation window in the first pass was  $32 \times 32$  pixels and in the second pass was  $16 \times 16$  pixels. Prior to processing, in order to improve accuracy, the raw images were tweaked to improve the contrast between the particles and background.

Lambda-2 criterion was used to capture the vortices due to its more accurate detection of the vortex centres when compared with other tested methods for the particular experiment (discussed by Coletta et al. 2019). The results went through two filters

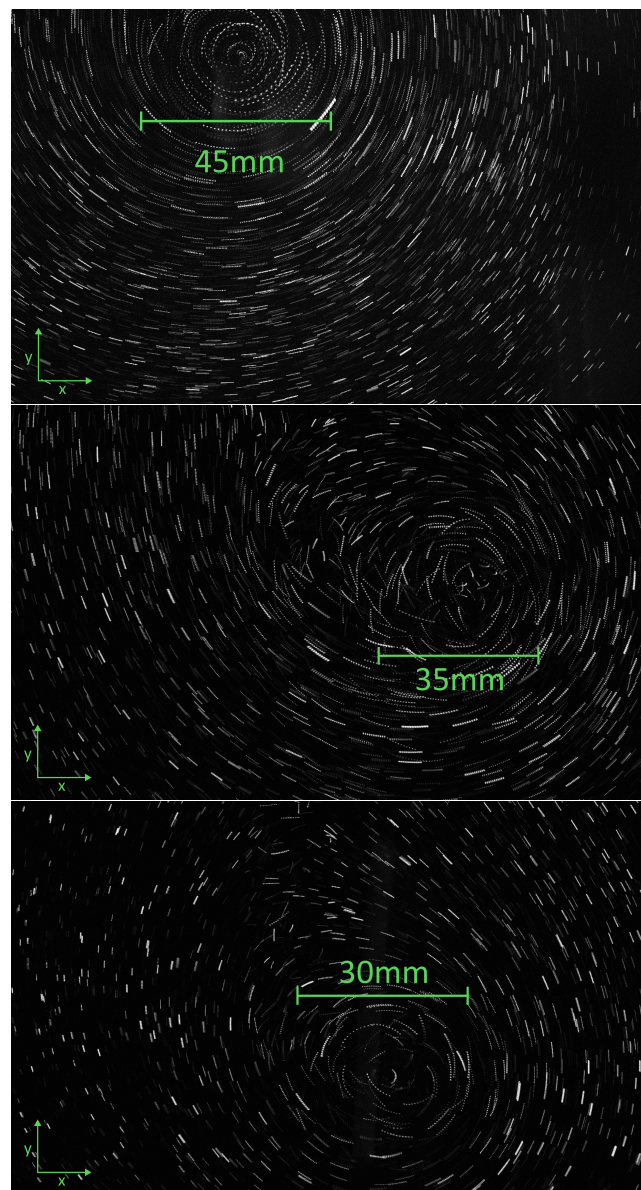


Figure 4: Flow visualisation of the vortices a) Clean  $30 \text{ cm s}^{-1}$ ,  $10^\circ$  b) Flexible extension  $30 \text{ cm s}^{-1}$ ,  $10^\circ$  c) Flexible extension  $20 \text{ cm s}^{-1}$ ,  $10^\circ$

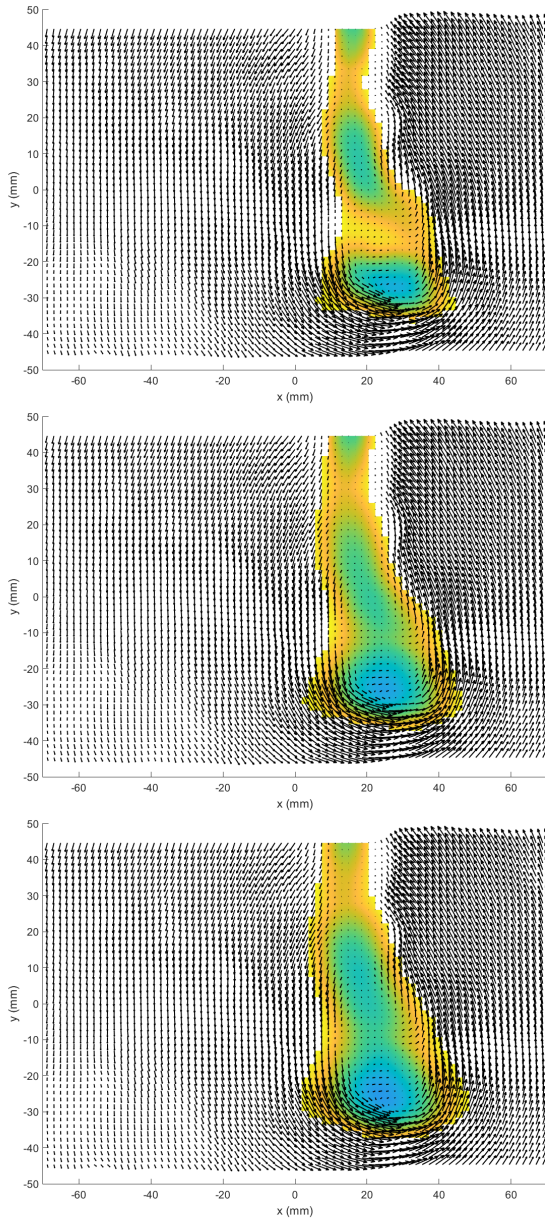


Figure 5: Code sensitivity to input vortex diameter a) 25 mm, b) 30 mm and c) 35 mm.

to remove erroneous vectors and finally any missing vectors were interpolated from the local mean. Only the contours  $> -0.2$  Lambda were plotted in order to remove the background noise in the flow field. Figure 5 demonstrates the sensitivity of the code to detecting the vortex cores when the user-defined vortex diameter is altered. Four potential cores can be observed in figure 5c where as the two central cores are harder to distinguish in figures 5a and b. The vortex diameter deemed appropriate for the case shown ( $30 \text{ cm s}^{-1}$ ,  $10^\circ$  angle of attack) from the diameter estimate extracted from the flow visualisation and the sensitivity test was 35 mm. It can be observed that the lower the defined diameter the more likely the code will detect erroneous vortex cores, with the opposite being true for increased diameters.

#### 4.5 Flow field

Due to confines of the test section size the wingtip had to accelerate from rest and stop within a short region therefore, they do not reach a steady condition until near the end of the traverse movement. With respect to this, due to the Wagner effect (Walker 1931), aerodynamic forces acting upon the wing are lower than if the wingtip was in a steady state, thus it can also be said that the roll up and vorticity off the flexible extensions are also lower. Despite this the test conditions for the clean and extension wingtips were identical and qualitative comparisons can be drawn between the two. The transition of each of the flexible extensions from an initial steady, stationary state to a developed cascade configuration can also be observed.

Figures 6, 7 and 8 show the effect of the flexible extensions on the vortex production over time, dependent on velocity and angle of attack. Figure 9 is the vortex development overtime with the extensions removed from the flow. In all cases the the vortex is dislocated further laterally and vertically away from the end of the wing due to the out of plane tip locations of the extensions. The shifting of the vortex compared to the reference (clean) case is beneficial in the reduction of induced drag as the wing is less effected, thereby improving span efficiency.

In each of the figures 6, 7, 8 and 9, where the elapsed time from the start of the run is  $t = 1.5s$ , the wingtips have fully exited the light sheet and the downstream effects are being observed. In the case of the flexible extensions the initially individually separated vortices begin to coalesce into a singular vortex at the tip location of the leading extension. The consistent merging of the vortices at

this location in each test pairs with the strength of the vortex produced off each extension's tip, which reduces for each extension moving aft. The short distance downstream in which the vortices combine are also attributed to the small spatial distance between each tip due to flexible extensions not reaching their steady state until the end of the traverse run. Therefore, the individual vortices are not as spread out and more easily amalgamate. To delay the larger vortex formation until later in the wake further adjustments to the lengths and inter-spacing of the flexible extensions can be made. It is also important to note in the configuration tested the wingtip extensions do not cover the entire chord length and therefore a vortex off the wing, all be it smaller than the clean configuration, is still present.

As would be expected for a wing section with no wingtip device, figure 9, shows the single larger vortex that is formed in the wake. When compared to figure 6 the vortex core off the clean wing is approximately 10 mm larger, suggesting the flexible extensions are providing a positive effect. The smaller vortex size indicates that the influence of induced drag is reduced, therefore implying an improved wing efficiency.

The flow patterns observed for the other angles of attack and flow velocities tested were comparable to the characteristics observed in the cases shown. The deflections of the extensions were proportional to the flow velocity and angle of attack, where the greater of either the conditions the larger the curvature and vertical displacement. As discussed previously the change in the leading extension tip location also changes the location of the formation of the combined vortex which can also be observed in the other tests. Conversely for the  $0^\circ$  angle of attack tests the flaplets had no deflection from their natural positions regardless of the traverse speed, which further confirms the relationship between lifting forces and curvature of the extensions.

The reducing effect of the flexible extensions as the angle of attack is decreased are supported by the findings of Berens 2008 and Cone 1962, which found that the induced drag reduction of a multi-winglet does not out way the profile drag penalty at small angles.

The separation of vortices formed off the wingtip extensions differ from those found by KleinHeerenbrink, Johansson, and Hedenström 2017 and Tucker 1993, in which the multiple vortices rotate around a common centre. The reason for the differences is thought to be due to two factors; the tests conducted herein were not in stable conditions

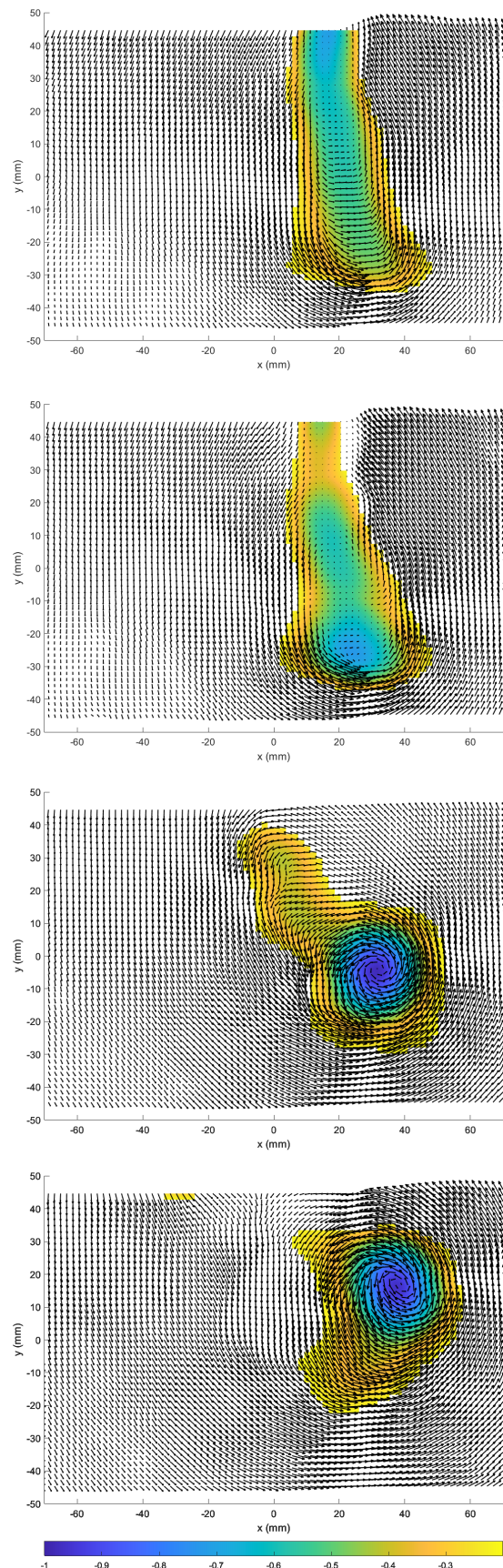


Figure 6:  $30 \text{ cm s}^{-1}$ ,  $10^\circ$  wingtip with flexible extensions at  $t=0.5s$ ,  $1s$ ,  $1.5s$  and  $3s$

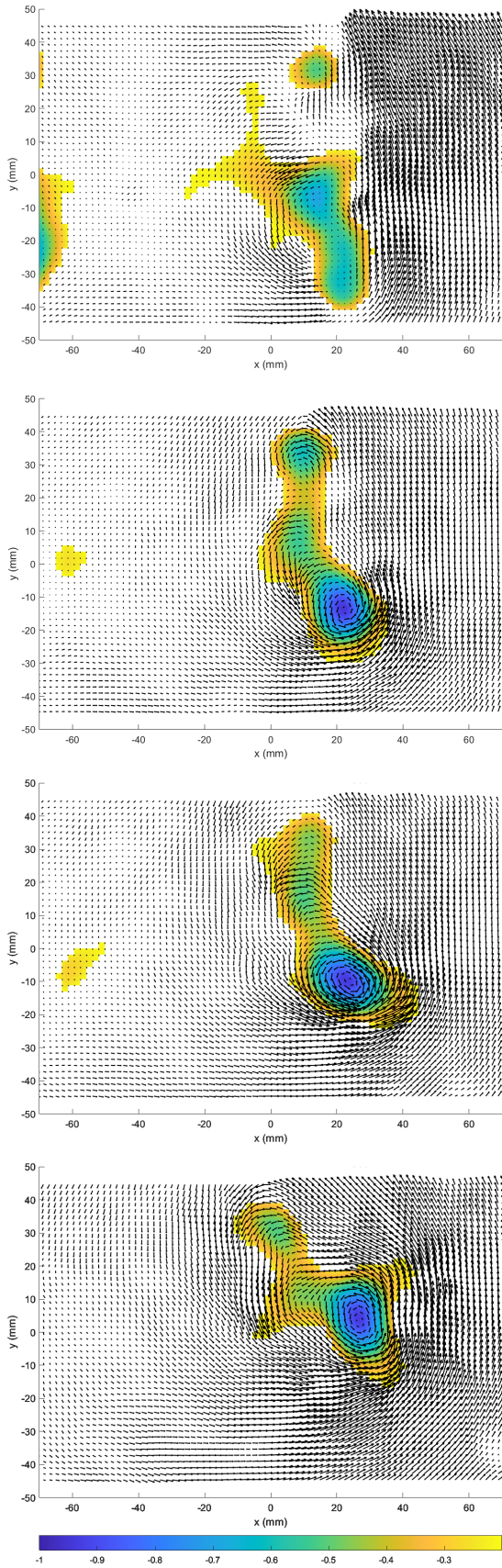


Figure 7:  $30 \text{ cm s}^{-1}$ ,  $5^\circ$  wingtip with flexible extensions at  $t=0.5\text{s}$ ,  $1\text{s}$ ,  $1.5\text{s}$  and  $3\text{s}$

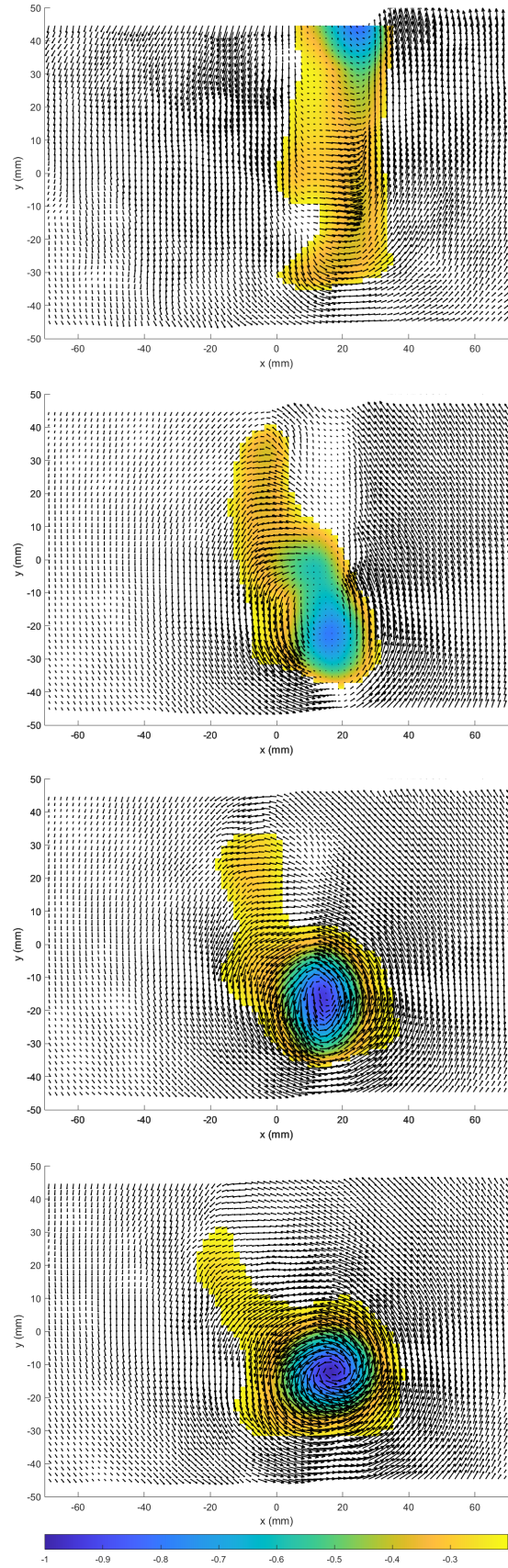


Figure 8:  $20 \text{ cm s}^{-1}$ ,  $10^\circ$  wingtip with flexible extensions at  $t=0.5\text{s}$ ,  $1\text{s}$ ,  $1.5\text{s}$  and  $3\text{s}$

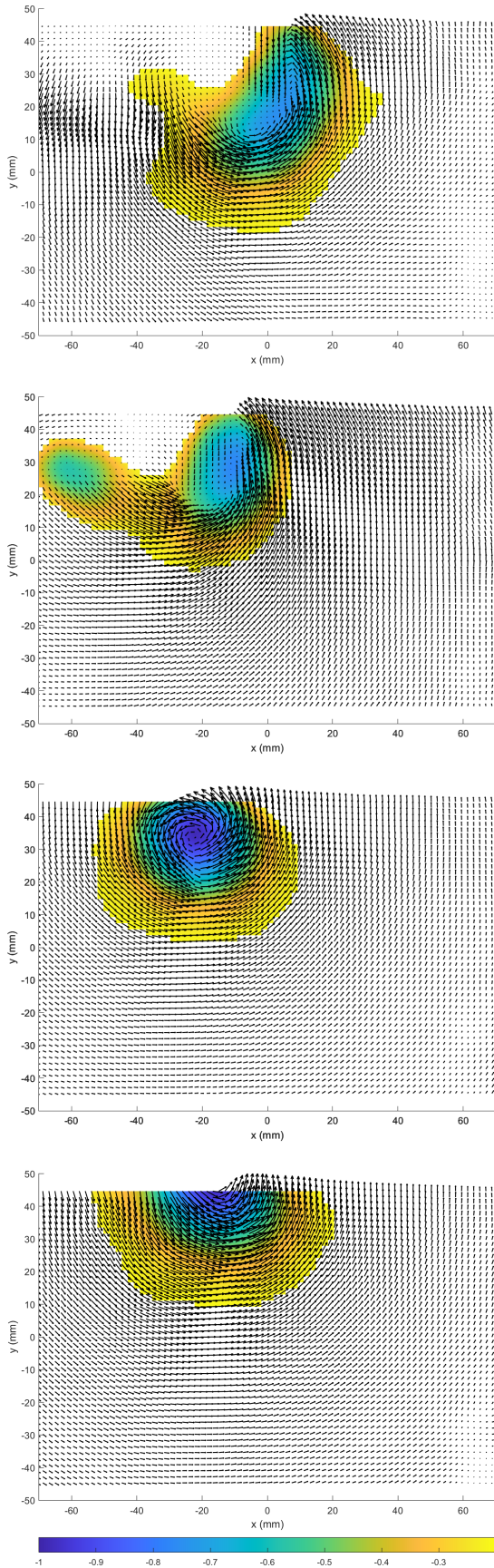


Figure 9:  $30\text{ cm s}^{-1}$ ,  $10^\circ$  clean wingtip at  $t=0.5\text{ s}$ ,  $1\text{ s}$ ,  $1.5\text{ s}$  and  $3\text{ s}$

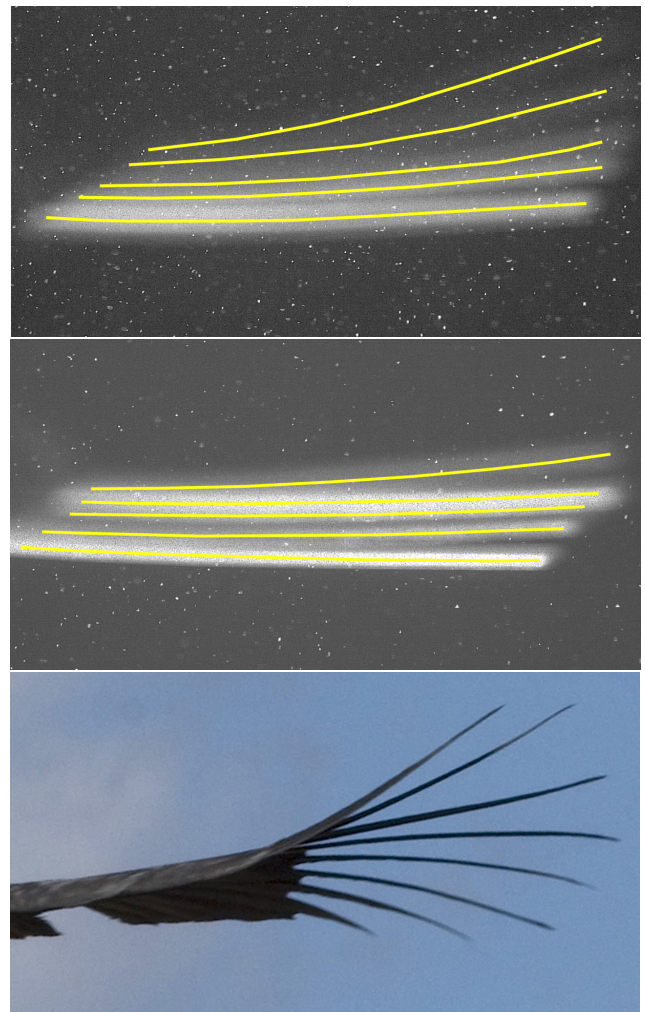


Figure 10: Configuration of flaplets at  $30\text{ cm s}^{-1}$  a)  $10^\circ$  and b)  $5^\circ$  angles of attack compared to that of a condor (Smith 2011)

meaning the tips of the flexible extensions had not fully separated resulting in the individual vortices being too close together and merging. Also in other studies, there is a greater horizontal tip displacement as opposed to just vertical displacement which would result in greater total separation and a common central point between tips.

#### 4.6 Natural configuration

Figure 10 shows the final stable position of the flexible extensions towards the end of the test run, the overlaid yellow lines are purely for ease of viewing. It is clearly identifiable that the increased angle of attack results in a higher curvature, in particular for the two leading wingtip extensions.

The increased curvature of the extensions at higher angles of attack suggest that the vertical separation between the tips is a function of the lift produced by the main wing and the wake off the preceding extension. This results in the cascading ef-

fect seen and is supported by the wake patterns observed on a flat plate at varying angles of attack (Shademan and Naghib-Lahouti 2020). It is assumed that the the wake off a single flexible extension is similar due to the induced local angle off attack caused by the roll up motion and free-stream flow. This implies the observed configuration is a result of the roll-up motion, preceding extensions wake and extension stiffness.

The flexible extensions can also be observed to replicate the cascading effect observed in nature despite the simplifications that were made. The main difference (ignoring the feathers deflecting downward) is the greater lateral separation between the tips found in nature than has been tested. However, particularly for the first three flexible extensions, similar curvatures can be seen on the feathers in the region that was being mimicked.

## 5 Conclusion

Flexible wingtip extensions mimicking a bird's slotted wingtip at  $20 \text{ cm s}^{-1}$ ,  $30 \text{ cm s}^{-1}$  and  $40 \text{ cm s}^{-1}$ , were tested at  $0^\circ$ ,  $5^\circ$  and  $10^\circ$  angle of attack have been shown to initially break up the strong vortex generated by a wing into smaller separated vortices. The modification to the vortex sheet has been shown in other studies (Tucker 1995) to reduce induced drag and therefore enhance efficiency. As the angle of attack is reduced, and in particular at  $0^\circ$  angle of attack, the extensions have a reduced effect due to the smaller roll-up off the wing. This study supports other similar findings from previous studies on the effects of a slotted wingtip and the separation of vortices that occur in both horizontal and vertical planes. This observation led to the conclusion of the flexible extensions to be self-adaptive dependent on the lift generated by the wing. Whereby the wake of the previous extension causes a reduced curvature of the proceeding extension. A further benefit from the addition of the flexible extensions is speculated to be quieter flight due to the separation of the vortices which are a large source of noise on aircraft, however this is not confirmed and yet to be tested.

## 6 Future work

As the ability of the flexible extensions have now been observed to be self-adaptive depending on the flow conditions and appear to mimic the slotted wingtips found in nature, testing can now be conducted in stable conditions. The configuration can

now be adjusted and optimised to further take advantage of the non-planar nature of the wingtip; this will be the next phase of study within our labs. Further studies on the interaction between the flaplets and a more definitive numerical experiment on the drag reduction are also left for future work.

## 7 Acknowledgements

The authors would like to acknowledge Keith Pamment for his assistance in manufacturing the mounting system for the wing. The position of Professor Christoph Bruecker is cofunded as the BAE SYSTEMS Sir Richard Olver Chair and the Royal Academy of Engineering Chair (grant RC-SRF1617/4/11) which is gratefully acknowledged.

## References

- Berens, B (2008). "Potential of Multi-Winglet Systems to Improve Aircraft Performance." PhD thesis. Technical University of Berlin. URL: <https://d-nb.info/990039978/34>.
- Coletta, M, F De Gregorio, A Visingardi, and G Iuso (2019). "PIV data: Vortex Detection and Characterization". In.
- Cone, C (1962). *The theory of induced lift and minimum induced drag of nonplanar lifting systems*. National Aeronautics and Space Administration.
- Cornell Lab of Ornithology (2019). "Peregrine Falcon". In: *All About Birds*. URL: [https://www.allaboutbirds.org/guide/Peregrine\\_Falcon/overview](https://www.allaboutbirds.org/guide/Peregrine_Falcon/overview) (visited on 05/20/2022).
- Dudley, D (2016). *Peregrine Falcon - A Juvenile Transitioning Into Adult Plumage?* URL: <https://www.featheredphotography.com/blog/2016/03/28/peregrine-falcon-a-juvenile-transitioning-into-adult-plumage>.
- KleinHeerenbrink, M, C Johansson, and A Hedenström (2017). "Multi-cored vortices support function of slotted wing tips of birds in gliding and flapping flight". In: *Journal of the Royal Society Interface* 14.130, p. 20170099.
- Schmitz, A, B Ponitz, C Brücker, H Schmitz, J Herweg, and H Bleckmann (2015). "Morphological properties of the last primaries, the tail feathers, and the alulae of *Acipiter nisus*, *Columba livia*, *Falco peregrinus*, and *Falco tinnunculus*". In: *Journal of morphology* 276.1, pp. 33–46.

- Shademan, M and A Naghib-Lahouti (2020). “Effects of aspect ratio and inclination angle on aerodynamic loads of a flat plate”. In: *Advances in Aerodynamics* 2.1, pp. 1–23.
- Smith, G (2011). *California Condor (Gymnogyps californianus) — Going through ... — Flickr*. URL: <https://www.flickr.com/photos/slobirdr/19467008269/>.
- Song, J, W Chen, D Yan, and S Guo (2021). “Study on drag reduction of flexible structure under flows”. In: *E3S Web of Conferences*. Vol. 245. EDP Sciences, p. 01019.
- Stanek, FJ (1965). “Free and Forced Vibrations of Cantilever Beams With Viscous Damping.” In: *Tech. Rep. June, National Aeronautics and Space Administration, Washington DC*.
- Tucker, V (1993). “Gliding birds: reduction of induced drag by wing tip slots between the primary feathers”. In: *Journal of experimental biology* 180.1, pp. 285–310.
- (1995). “Drag reduction by wing tip slots in a gliding Harris’ hawk, *Parabuteo unicinctus*”. In: *The Journal of experimental biology* 198.3, pp. 775–781.
- Walker, PB (1931). “Growth of circulation about a wing and an apparatus for measuring fluid motion”. In: *ARC report*.
- Williams, D (2019). “The Apollo 15 Hammer-Feather Drop”. In: *NASA*. URL: [https://nssdc.gsfc.nasa.gov/planetary/lunar/apollo\\_15\\_feather\\_drop.html](https://nssdc.gsfc.nasa.gov/planetary/lunar/apollo_15_feather_drop.html) (visited on 05/20/2022).
- Wissa, A, A Han, and M Cutkosky (2015). “Wings of a feather stick together: morphing wings with barbule-inspired latching”. In: *Conference on Biomimetic and Biohybrid Systems*. Springer, pp. 123–134.
- Withers, PC (1981). “The aerodynamic performance of the wing in red-shouldered hawk BUTEO lznearzs and a possible aeroelastic role of wing-tip slots”. In: *Ibis* 123.2, pp. 239–247.